ELSEVIER

Journal of Nuclear Materials 290–293 (2001) 623–627

journal of nuclear materials

www.elsevier.nl/locate/jnucmat

Impurity behavior before and during the *x*-point MARFE in JT-60U

S. Higashijima *, H. Kubo, T. Sugie, T. Nakano, S. Konoshima, H. Tamai, K. Shimizu, A. Sakasai, N. Asakura, S. Sakurai, K. Itami

Japan Atomic Energy Research Institute, Naka Fusion Research Establishment, 801-1 Mukouyama, Naka-machi, Naka-gun, Ibaraki-ken 311-0193, Japan

Abstract

The divertor geometry of JT-60U was modified in 1998 to add a pumping slot near the outer strike point for improved pumping. In the both-side pumping divertor, the *x*-point MARFE onset density is ~10% higher with pumping than without pumping. Radiated power near the *x*-point is decreased by pumping, and the divertor pumping is effective in suppression of the *x*-point MARFE. The effect of outer pumping is investigated in L-mode plasmas. The onset densities of the *x*-point MARFE are the same in both divertors. The fraction of total radiated power over absorbed power at the *x*-point MARFE onset is ~20% higher in the both-side pumping divertor than in the inside pumping divertor, but it does not depend on the onset density and on a distance between the private dome and the outer leg. Carbon penetration from the divertor region to the main plasma has a weak dependence on the gap-out in the both-side pumping divertor.

Keywords: MARFE; JT-60U; Divertor; Divertor geometry; Impurity screening

1. Introduction

Cold and dense divertor plasmas are necessary for next generation devices, such as ITER, to reduce erosion of divertor plates. The appearance of the *x*-point MARFE, however, must be avoided because it causes an increase of impurity density in main plasmas. For this purpose, the divertor was modified in various machines, and the effect of divertor geometry [1–4] and the effect of puffing and pumping [5–8] have been investigated.

In JT-60U, the divertor geometry was modified in 1997 from an open divertor to a w-shaped pumped divertor to demonstrate cold and dense divertor operation [9]. The following three results were obtained after this modification; (1) reduction of the H-mode threshold power [10], (2) prevention of chemically sputtered hydrocarbon molecules from easily reaching the *x*-point and penetrating the main plasma across the separatrix by the private dome (dome effect) and (3) reduction of carbon impurity in the main plasma by gas puffing from the main plasma and divertor pumping (puff & pump effect) [11,12]. In 1998, a pumping slot was added near the outer strike point. The aim of this re-modification is to improve the pumping efficiency in the high density range so that particle flux increases in the outer divertor.

The objective of this paper is to investigate the following two subjects: (1) the advantage of improved pumping, and (2) the difference in carbon impurity behavior between the inside pumping divertor and the both-side pumping divertor. In the re-modified divertor, it is expected that the carbon concentration in the main plasma decreases in the both-side pumping divertor compared with that in the inside pumping divertor by the combination of gas puffing and improved divertor pumping. We consequently compare carbon density in the main plasma, radiated power fraction, carbon penetration from the divertor region to the main plasma in NB-heated L-mode plasmas.

* Corresponding author. Tel.: +81-29 270 7349; fax: +81-29 270 7419.

E-mail address: higashij@naka.jaeri.go.jp (S. Higashijima).

0022-3115/01/$ - see front matter
PII: S0022-3115(00)00518-3

In this paper, we present the re-modified divertor and diagnostics of JT-60U in Section 2. In Section 3, we demonstrate the disappearance of the x-point MARFE by pumping. Finally in Section 4, an effect of the both-side pumping divertor on carbon impurity in the L-mode plasmas is presented.

2. Divertor geometry and diagnostics

Fig. 1 shows the geometry of w-shaped both-side pumping divertor, pumping path to cryo-pumps, diagnostics and plasma configuration in the divertor. The divertor consists of inner and outer baffle plates, divertor target tiles, a private dome and two toroidally continuous pumping slots. In the inside pumping divertor, a toroidally continuous pumping slot near the outer leg did not exist. In the both-side pumping divertor, particles are exhausted through the two pumping slots near the inner and the outer leg in the private flux region. Particles from the inner leg side are conducted under the divertor dome, under outer baffles and led to three cryo-pumps with particles from the outer leg side. When the neutral pressure is different between the inner and outer divertor, a flow of neutral particle is generated. The particle flow from the inner private region to the outer private region under the private dome is predicted when the divertor detaches in the inner leg side. However, a large increment of neutral pressure in outer leg side was not measured with the fast-response ion gauges. When we enclose deuterium gas of 0.1 Pa in the vacuum vessel and estimate the decay of D_2 pressure by pumping, the pumping efficiency is about 25% higher with both-side pumping than with inside pumping (from 12.7 to 15.9 Pa m^3/s).

The spatial emission profiles of deuterium and carbon in the divertor are measured with two optical fiber arrays. A 60-channel optical fiber array measures horizontal spatial emission profiles [13]. In this paper, CD-band (wavelength: ~430.5 nm), C II (657.8 nm), C IV (580.1 nm) and D_α (656.1 nm) intensities are measured. A 32-channel optical fiber array measures vertical spatial emission profiles of one wavelength by an interference filter. Intensities are measured for the same spectral lines for the horizontal 60-channel optical fiber array. However, the S/N ratio of C IV intensity with a 32-channel optical fiber array was too small to estimate C IV behavior.

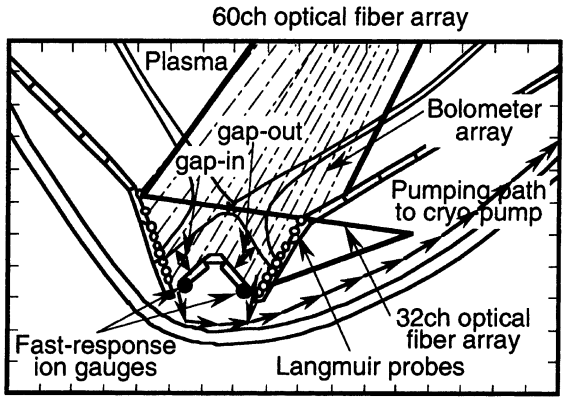

Fig. 1. W-shaped both-side pumping divertor and diagnostics. A row of arrows shows a pumping path.

A bolometer array viewing from the top of the main plasma [14] measures horizontal profiles of radiated power (13 channels), and this is used to judge the appearance of the x-point MARFE. Two fast-response ion gauges [15] measure neutral pressure at the inner and outer pumping slots. Eighteen Langmuir probes are installed in a poloidal divertor section. The measured ion saturation current is used for determinating the divertor detachment.

3. Suppression of x-point MARFE by divertor pumping

After the re-modification of the divertor, the gas puffing rate to keep a constant density increases with a decrease of gap-out in comparison with that before the re-modification [16]. Here, the gap-out is defined as a distance between the private dome and the outer leg. In the both-side pumping divertor the onset density of the x-point MARFE with pumping is ~10% higher than without pumping. We try to keep the density between the onset density of the x-point MARFE with pumping and that without pumping by feedback control and to demonstrate that the x-point MARFE disappears by pumping. The original aim of this experiment is to understand the mechanism of the x-point MARFE generation.

This experiment is carried out in L-mode plasmas. The discharge condition was as follows; plasma current (I_p) = 1.5 MA, toroidal field (B_t) = 3.5 T, injected power of NBI (P_{NB}) ~ 4 MW, plasma volume (V_p) ~ 70 m^3, gas puffing from the top of main plasma, a distance between the inner leg and the private dome (gap-in) ~2 cm and gap-out ~2 cm.

Fig. 2 shows the time evolution of a discharge with pumping started after the x-point MARFE appearance. The time evolutions of ion saturation current (I_s) and radiation in the divertor are shown in Fig. 3. Plasma configuration is fixed at 4 s, and NBI is injected at 5 s. The line averaged density ($\bar{n}_e$) is kept constant from 7.8 s by feedback control. D_α emission near the inner strike point decreases from ~7.6 s, and the inner divertor is partially detached. The inner strike point is located between two probes (channel 8 and 9 in Fig. 3(a)). At ~7.6 s, I_s (9 ch) in the private flux region decreases and I_s (8 ch) above the inner strike point increases simulta-

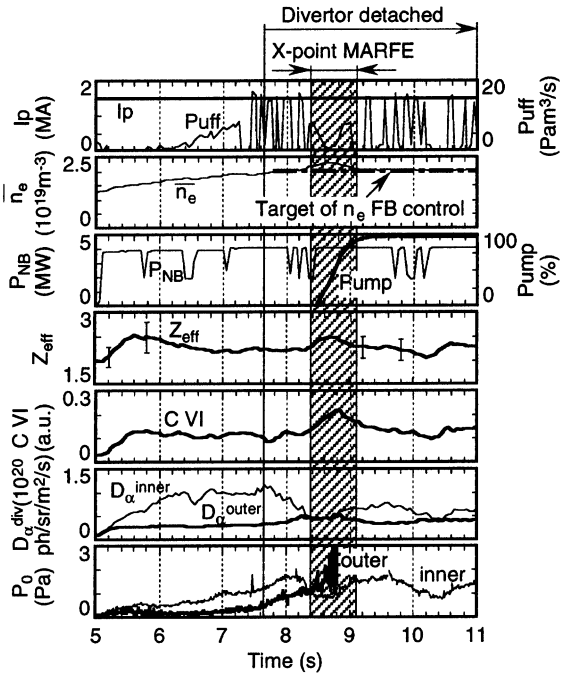

Fig. 2. Time evolution of plasma current, gas puffing rate, electron density, injected power of NBI, the percentage of divertor pumping, Z_{eff}, C VI emission, D_α emissions near the inner and outer strike points and neutral pressures in the inner and outer divertor. Neutral pressure in the inner divertor is not available during the x-point MARFE because of saturation.

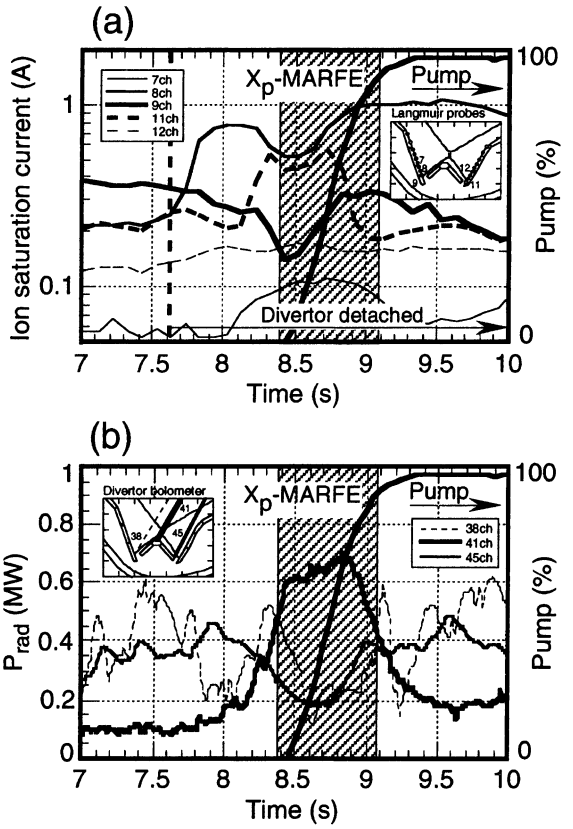

Fig. 3. Time evolutions of: (a) ion saturation current; and (b) divertor radiation.

neously. I_s (8 ch) decreases from ~8.1 s, and the inner divertor is deeply detached. At the same time, I_s (11 ch) near the outer strike point increases, and recycling increases in the outer divertor. Then I_s (11 ch) near the outer strike point decreases from ~8.3 s and the outer divertor is partially detached. The radiation profile peaks near the x-point from ~8.4 s, indicating the onset of the x-point MARFE. When the x-point MARFE appears, particle fluxes from the main plasma become larger in the outer divertor than in the inner divertor, as shown by D_α emissions and neutral pressures. During the x-point MARFE, the density becomes higher and carbon impurity increases because the edge temperature decreases and particles from the divertor region can easily enter the main plasma.

The time evolution of the x-point MARFE is faster than a typical time resolution of diagnostics because the x-point MARFE is a thermal instability. However, it is expected that we can investigate the x-point MARFE disappearance because neutral pressure at the strike points can be decreased gradually by pumping. After the divertor pumping is turned on, I_s (8 ch) and I_s (11 ch) near both strike points increase immediately, and the current at outer strike point decreases from ~8.75 s. Z_{eff} decreases from ~8.8 s. These observations show that the inner divertor change to the partially detached divertor because I_s (8 ch) is kept on ~1 A. At last, radiation near the x-point decreases from ~8.9 s, and the x-point MARFE, exhibiting itself as a peak of divertor radiation profile near the x-point, disappears at ~9.1 s. This experiment suggests that the divertor pumping is a control tool to suppress the x-point MARFE.

4. Comparison of carbon behavior between the inside and both-side pumping

This experiment is carried out in L-mode plasmas with the following conditions, $I_p = 1.2$–1.5 MA, $B_t = 3.5$ T, $V_p \sim 70$ m^3, $P_{NB} \sim 4$ MW, deuterium gas puffing from the top of the main plasma, divertor pumping. The density is gradually increased up to the x-point MARFE onset density by the feedback control. The gap-in is fixed in the range from 2.5 to 4.5 cm and the gap-out is scanned.

The fraction of total radiated power over absorbed power is investigated. The dependence on the gap-out

and on the normalized onset density of x-point MARFE is shown in Fig. 4. Here, the onset density of x-point MARFE is normalized by the Greenwald density. This fraction is ~20% higher in the both-side pumping divertor than in the inside pumping divertor, but it does not depend on the gap-out and on the normalized onset density.

The onset density of x-point MARFE is not clearly difference between the inside the both-side pumping. Z_{eff} just before the x-point MARFE onset in the both-side pumping divertor is higher than in the inside pumping divertor. However, these parameters depend on the wall condition. Therefore, carbon penetration from the divertor region to the main plasma is estimated and compared between the inside and both-side pumping. Fig. 5 shows the penetration factor of carbon, $\eta = (n_{\mathrm{C}}^{\mathrm{main}}/n_{\mathrm{D}}^{\mathrm{main}})/(\Gamma_{\mathrm{C}}^{\mathrm{div}}/\Gamma_{\mathrm{D}}^{\mathrm{div}})$, at the density of ~40% Greenwald density. Here, $n_{\mathrm{C}}^{\mathrm{main}}, n_{\mathrm{D}}^{\mathrm{main}}, \Gamma_{\mathrm{C}}^{\mathrm{div}}$ and $\Gamma_{\mathrm{D}}^{\mathrm{div}}$ show carbon density and deuterium density in the main plasma, and carbon influx and deuterium influx in the divertor, respectively. Carbon density in the main plasma is estimated from Z_{eff} value and impurity signals measured with a VUV spectrometer. To estimate the influx, the electron temperature in divertor is assumed to be ~20 eV and the S/XB values [17], representing the ionization events per photon, of C II and D_α emissions are used. The penetration factor of carbon in the both-side pumping divertor has a weak dependence on the gap-out in the range of gap-out $\leqslant$4 cm although the error bars are large. It shows that the both-side pumping is effective in decreasing carbon impurity in the main plasma. However, as the effect of improved pumping is small in L-mode plasmas, we try to compile the H-mode data and to develop the effect.

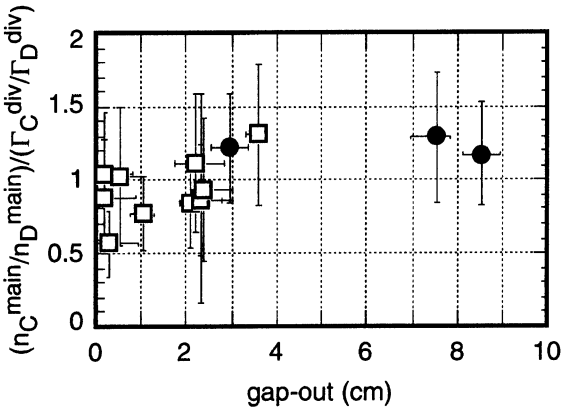

Fig. 5. The gap-out dependence of carbon penetration from divertor region to main plasma. Closed circles (●): inside pumping and open squares (□): both-side pumping.

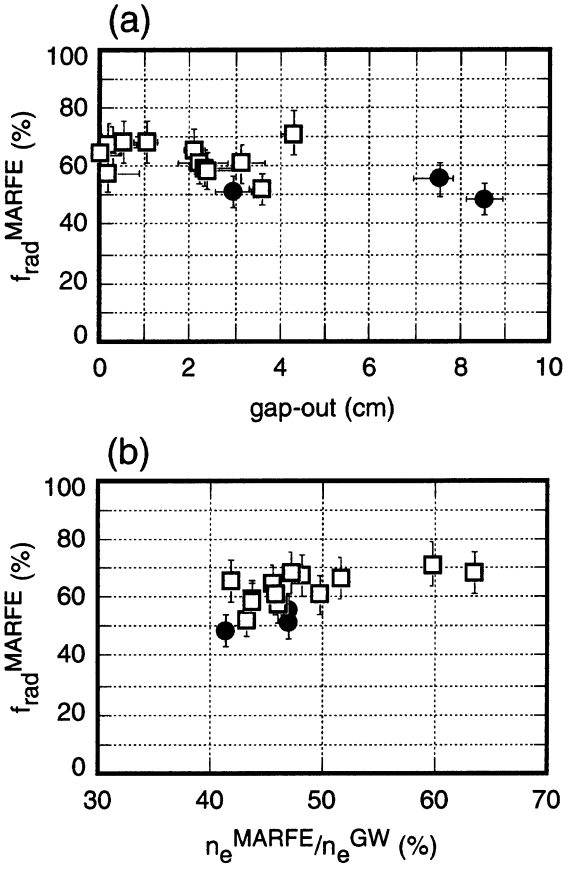

Fig. 4. (a) The gap-out dependence of the radiation fraction. (b) The dependence of the fraction on the normalized onset density of the x-point MARFE. Closed circles (●): inside pumping and open squares (□): both-side pumping.

5. Summary

The carbon impurity behavior is investigated in the both-side pumping divertor of JT-60U. The conclusions are summarized as follows:

- The onset density of the x-point MARFE is ~10% higher by pumping in the both-side pumping divertor. It is demonstrated that the x-point MARFE can be eliminated by divertor pumping. Pumping is thus an efficient control tool.
- The radiated power fraction from the plasma just before the x-point MARFE is ~20% higher in the both-side pumping divertor than in the inside pumping divertor, but it does not depend on the gap-out and on the normalized onset density.
- The penetration factor of carbon impurity decreases with the gap-out in the range of gap-out $\leqslant$4 cm, but the effect of puffing and improved pumping on shielding is small in L-mode plasmas.

Acknowledgements

The authors are grateful to the JT-60 team for excellent cooperation. The authors would like to thank Drs R. Yoshino, H. Ninomiya and A. Funahashi for continuous support.

References

[1] G.C. Vlases et al., J. Nucl. Mater. 266–269 (1999) 160.
[2] S.L. Allen et al., J. Nucl. Mater. 266–269 (1999) 168.
[3] R. Schneider et al., J. Nucl. Mater. 266–269 (1999) 175.
[4] H.-S. Bosch et al., Plasma Phys. Control Fus. 41 (1999) A401.
[5] M.J. Schaffer et al., Nucl. Fus. 35 (1995) 1000.
[6] M.A. Mahdavi et al., J. Nucl. Mater. 220–222 (1995) 13.
[7] A. Kallenbach et al., Nucl. Fus. 35 (1995) 1231.
[8] H.-S. Bosch et al., Phys. Rev. Lett. 76 (1996) 2499.
[9] N. Hosogane et al., in: Proceedings of the 16th International Conference on Plasma Physics and Control Nuclear Fusion Research, Montreal, vol. 3, IAEA, Vienna, 1996, p. 555.
[10] T. Fukuda et al., Plasma Phys. Control. Fus. 42 (2000) A289.
[11] S. Higashijima et al., J. Nucl. Mater. 266–269 (1999) 1078.
[12] N. Hosogane et al., in: Proceedings of the 17th International Conference on Plasma Physics and Control Nuclear Fusion Research, Yokohama, vol. 3, IAEA, Vienna, 1999, p. 903.
[13] H. Kubo et al., Plasma Phys. Control. Fus. 37 (1995) 1133.
[14] T. Ishijima et al., Plasma Phys. Control. Fus. 41 (1999) 1155.
[15] H. Tamai et al., J. Nucl. Mater. 266–269 (1999) 1219.
[16] A. Sakasai et al., these Proceedings.
[17] J. Roth et al., Suppl. Nucl. Fus. 1 (1991) 64.